

pubs.acs.org/cm Article

Seeded Growth of Nanoscale Semiconductor Tetrapods: Generality and the Role of Cation Exchange

Michael J. Enright, Florence Y. Dou, Shenwei Wu, Emily J. Rabe, Madison Monahan, Max R. Friedfeld, Cody W. Schlenker, and Brandi M. Cossairt*



Cite This: Chem. Mater. 2020, 32, 4774-4784



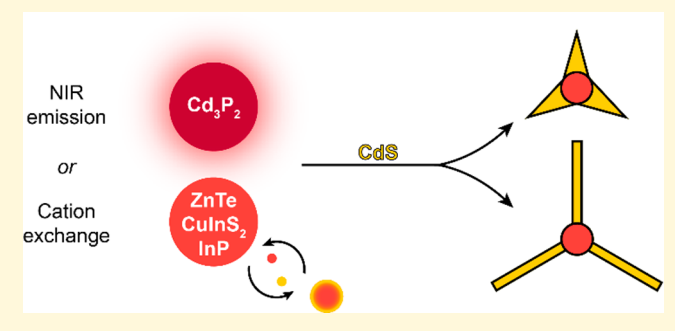
ACCESS

III Metrics & More

Article Recommendations

s Supporting Information

ABSTRACT: Nanoscale tetrapods were synthesized with independently tunable core and arm sizes and aspect ratios from a spectrum of quantum dot seeds, including ZnTe, CuInS₂, InP, InP/ZnS, and Cd₃P₂. The range of II–VI, I–III–VI, III–V, and II–V seeds included both cubic and tetragonal lattices, demonstrating the versatility of CdS arm growth upon surfaces with accessible (111) planes, including those with distorted those with distorted structures. Except for the Cd₃P₂ seeds, where the effect is inconsequential, cation exchange in the core was observed to occur concurrently with arm growth to give alloyed cores in the final tetrapods. This result supports recent work characterizing the



composition of core/shell quantum dots composed of distinct cations and presents a challenge to achieving clean interfaces in nanoscale semiconductor heterostructures grown by using traditional solvothermal methods. Conversely, the robust Cd_3P_2/CdS tetrapod architecture represents a rare example of near-infrared (NIR) emission in a multipod heterostructure. NIR-emissive tetrapod heterostructures were successfully obtained from Cd_3P_2 cores in combination with both high and low aspect ratio CdS arms.

■ INTRODUCTION

The synthesis of nanomaterials of various shapes and sizes is well established, and the importance of size and structure tunability is comprehensively understood. 1–14 However, methodologies for assembling multicomponent heterostructures with independently tunable components are less ubiquitous. Despite heterostructure design being an ideal strategy to tune charge carrier localization and enhance the function of semiconductor nanomaterials, synthetic techniques to access a broad spectrum of material combinations with independently customizable dimensions are currently underdeveloped. In addition to being practically useful in the fabrication of optoelectronic devices, heterostructure design is also foundational to developing a more robust, fundamental understanding of charge localization in complex systems.

The simplest and most well-studied heterostructure is the spherical core/shell motif.^{20–24} These systems have an outer shell that serves as a protective layer capable of passivating surface traps and defects to enhance luminescence.^{25–32} Consequently, core/shell structures have become important luminescent materials across a spectrum of advanced technologies, including displays, solid-state lighting, and biological imaging.^{8,24,33,34} However, while the core/shell motif is a leading architecture for enhancing emission,^{34–36} this structure presents several disadvantages for applications where charge extraction is necessary, such as photocatalysis. In

a core/shell system, the handles for modulating the optoelectronic properties are limited since core size and shell thickness are the primary tunable parameters. ^{24,34,37,38} Furthermore, increasing shell thickness inhibits the ability to regenerate charge carriers within the core using external chemical reagents or an applied electrochemical potential. ^{39–41} This can lead to undesirable effects such as unsuccessful catalytic turnover or photodegradation. ^{42–44}

Dot-in-rod and rod-rod heterostructures begin to address these challenges by having exposed or nominally shelled faces to enable more efficient quenching of charge carriers after separation. Within these motifs, the rod length and location of the dot or seed can be controlled. The width of the rod, however, is determined by the width of the seed with a limited number of exceptions. Moreover, 1-D nanostructures require a wurtzite crystal seed to serve as a scaffold for rod elongation, and many nanomaterials do not have easily accessible wurtzite crystal phases by colloidal synthetic approaches. Composition variation in semi-

Received: April 1, 2020 Revised: May 5, 2020 Published: May 6, 2020





conductor nanorods achieved via cation exchange broadens the number of accessible products; however, wurtzite-related crystal structures are once again necessary.⁵⁴ Thus, the spectrum of material combinations and the tunability of dotin-rod and rod-rod architectures are limited to materials with accessible wurtzite crystal phases.

Tetrapod assemblies represent a potentially versatile heterostructure configuration capable of addressing the shortcomings of 0-D and 1-D structures. One major advantage of the tetrapod architecture is the customizability of the cubic phase seed. A wide variety of nanomaterials can be straightforwardly synthesized in the cubic phase with tunable sizes to serve as cores. ^{55–57} In addition to controlling the size of the core, both the arm length and width can also be modified, even independently of the core size. ^{17,58,59} Furthermore, both the exposed arm or nominally shelled core components may be accessible to enable charge carrier replenishment in type II heterostructures.

Most tetrapod studies focus exclusively on materials from the II–VI family. ⁶⁰ Initial tetrapod syntheses were products of polytypism in which the small energy difference between cubic and wurtzite phases (>10 meV) enabled initial nucleation of zinc blende spherical cores followed by elongation of wurtzite arms upon each core's (111) facets. ^{13,59,61,62} Seeded growth approaches, especially in the case of CdSe/CdS, have received a significant amount of attention for their tunable optoelectronic properties and greater synthetic control over yield and tetrapod morphology when separating the core and arm synthetic steps. ^{8,16,63,64} The seeded tetrapod growth approach gives access to greater structural complexity by expanding the narrow window of synthetic conditions, such as temperature, ligand concentration, and precursor amount. However, even CdSe/CdS tetrapod systems are inherently limited to a narrow range of overall energetics, toggling between type I and quasitype II systems. ^{65–68}

In theory, seeded tetrapod architectures should be accessible from any seed with accessible (111) faces for (0001) wurtzite arm elongation. 59,69 The ideal criteria for a generalizable synthetic route to tetrapod heterostructures are twofold: the ability to use any material combination to assemble heterostructure tetrapods and the ability to individually control the size and shape of each subcomponent. These ultimately enable fine-tuning of the heterostructure's optoelectronic properties. This should apply to seeded growth of wurtzite II-VI materials upon III-V, I-III-IV, and II-V systems. Thus far, reports of ZnTe/CdS, CuInS₂/CdS, and InP/ZnS/ CdS have been documented. 63,64,70,712 However, it is also known that cation exchange between cadmium and indium, copper, or zinc in chalcogenide lattices is readily facilitated under typical nanomaterial growth conditions.^{72–74} In light of cation exchange, a primary goal of this work was to re-examine tetrapod growth in known systems and expand the range of accessible tetrapod products beyond the II-VI system.

First, we present a versatile synthetic approach to obtain tetrapod nanostructures with tunable arm dimensions from a spectrum of seeds (ZnTe, CuInS₂, and InP). Despite these seeds serving as scaffolds for tetrapod synthesis, we found that many cores are highly susceptible to cation migration and exchange. We explored the impacts of cation diffusion within a model tetrapod assembly system formed from InP/ZnS core/shell seeds. Despite retaining a phosphide lattice at the core to serve as a scaffold for tetrapod arm growth, cation exchange could not be fully mitigated. Finally, we have demonstrated the

first near-IR emissive tetrapods synthesized from II–V seeds while tuning the size and shape of the core and arm components independently of one another.

■ EXPERIMENTAL SECTION

Materials. All glassware was dried in an oven overnight at 160 °C before use. All manipulations were performed by using standard Schlenk or glovebox techniques under dry N₂. Zinc acetate (99.99%), zinc chloride (99.99%), zinc stearate (technical grade), cadmium oxide (CdO, 99.9%), cadmium chloride (99.99%), cadmium acetate (Cd(OAc)₂, 98%), indium acetate (99.99%), indium chloride (98%), copper iodide (>99.5%), metallic tellurium (Te, 99.997%), selenium (Se, 99.999%), sulfur (S, 99.5%), superhydride (LiBH(CH₂CH₃)₃) solution in THF (1 M), tris(diethylamino)phosphine (97%), trioctylphosphine (TOP, 97%), octylamine (99%), oleic acid (OA, 90%), myristic acid (≥99%), dodecanethiol (98%), and oleylamine (70%) were purchased from Sigma-Aldrich and used as received without further purification. Octadecylphosphonic acid (ODPA, 99%) was purchased from PCI Synthesis and used as received. 1-Octadecene (ODE, 90%) was purchased from Sigma-Aldrich and distilled prior to use. Trioctylphosphine oxide (TOPO, 90%) was purchased from Sigma-Aldrich and twice recrystallized from acetonitrile until no impurities remained by 31P and 1H NMR spectroscopy. Methanol, ethanol, 2-propanol, acetonitrile, ethyl acetate, toluene, and pentane were purchased anhydrous and/or dried over CaH2 and stored over 3 Å molecular sieves prior to use. P(SiMe₃)₃ was synthesized as reported previously.

Synthesis of CdSe Quantum Dots (QDs). CdSe QDs were prepared according to a literature procedure. To P=Se was prepared by dissolving 0.060 g of Se in 0.84 g of TOP (1.01 mL) and 4.16 mL of ODE until the solution turned completely clear. Next, 0.134 g of CdO, 1.20 mL of OA, and 8.00 mL of ODE were added to a 50 mL three-neck flask. The mixture was degassed for 30 min at room temperature before heating to 240 °C under N_2 . Once the cadmium solution was completely clear (5–10 min, indicating formation of cadmium oleate), 5 mL of TOP=Se was injected rapidly. Particles with a diameter of 4.0 nm were obtained by quenching the reaction (removing the heating mantle) after ~5 min. The nanocrystals were purified by repeated precipitation/resuspension in MeOH and toluene five times. The first two precipitation steps required ethyl acetate as a cosolvent to remove ODE.

Synthesis of ZnTe QDs. ZnTe QDs (8 nm) were synthesized by using a modified literature procedure. 72 In a 50 mL three-neck flask, 0.26 g (1.4 mmol) of zinc acetate was mixed with 4 mL (12.7 mmol) of OA and 20 mL of 1-ODE. The mixture was degassed for at least 30 min before being heated to 200 °C under N2. After 1 h a clear solution formed, and the temperature was dropped to 160 °C. The Te precursor was prepared by adding 1.6 mL of superhydride solution (1 M in THF) and 2 mL of oleylamine to 1.0 mL of TOP=Te (1.0 M Te in TOP). This tellurium precursor was stirred for 1 h at room temperature until the solution became homogeneous and subsequently injected rapidly into the zinc solution at 160 °C. The temperature was increased to 190 °C and maintained for 60 min before quenching the reaction by cooling to room temperature. Excess solvent and volatile organics were removed by vacuum distillation at 180 °C. The ZnTe nanorods were purified by repeated precipitation/ resuspension in EtOH and pentane five times. The resulting ZnTe QDs have an aspect ratio of 2. Note of comparison to other procedures: similar procedures have been used to give ZnTe nanorods with aspect ratios of ≥ 3 . The present synthesis stirred the tellurium precursor for longer times (1 h as opposed to 20 min), and vacuum distillation was performed at a higher temperature (180 °C vs 150 °C).

Synthesis of Copper Indium Sulfide QDs. CIS-QDs were synthesized by using a literature procedure. First, 73 mg (0.25 mmol) of indium acetate, 47.5 mg (0.25 mmol) of copper iodide, and 4 mL of dodecanethiol were added to a 50 mL three-neck flask. The flask was purged with N_2 for 30 min and subsequently heated while stirring to 120 °C over 20 min. The solution was maintained at 120

 $^{\circ}$ C for an additional 10 min, until a clear yellow solution was formed. The solution was then heated to 230 $^{\circ}$ C and gradually changed color from yellow to dark red. After refluxing for a set time (1–30 min), the reaction was quenched by removing the flask from heat.

Synthesis of InP Spherical QDs. Indium phosphide QDs were synthesized via a two-step synthetic procedure reported previously. Briefly, 0.93 g (3.20 mmol) of indium acetate and 2.65 g (11.6 mmol) of myristic acid were heated under vacuum at 100 °C in a 100 mL three-neck flask for 12 h to generate indium myristate. After indium myristate was formed, the apparatus was placed under N2, and 20 mL of toluene was added. This solution was heated to 110 °C, and a mixture of 465 μ L of tris(trimethylsilyl)phosphine (P(SiMe₃)₃) and 10 mL of toluene was quickly injected to form InP magic size clusters (MSCs). InP MSC formation was monitored by UV-vis absorbance until no changes were observed. Purification of MSCs was achieved by repeated precipitation with acetonitrile and resuspension in toluene. For storage, solvent was removed, and MSCs were stored dry in glovebox. To obtain 3.0 nm InP QDs, 200 mg of MSCs was dissolved in 2 mL of ODE and injected into a N2-purged 100 mL three-neck flask with 38 mL of additional ODE at 270 °C. Growth for 20 min yielded 3.0 nm InP nanoparticles. Excess ODE was removed by vacuum distillation at 150 °C, and QDs were purified by multiple resuspension in toluene and precipitation with ethanol.

Synthesis of InP/ZnSeS QDs. InP/ZnSeS core/shell QDs were prepared according to a previous report. Prince State Companies of the prepared according to a previous report. Prince State Companies of the prepared according to a previous report. State Companies of the prepared according to a previous report. State Companies of the prepared according to a previous report. State Companies of the prepared according to a previous report. State Companies of the prepared according to a previous report. State Companies of the prepared according to a previous report. State Companies of the prepared according to a previous report. State Companies of the prepared according to a previous report. State Companies of the prepared according to a previous report. State Companies of the prepared according to a previous report. State Companies of the prepared according to a previous report. State Companies of the prepared according to a previous report. State Companies of the previous report report. State Companies of the previous report report. State Companies of the pr dissolved in 1 mL of ODE and injected into a N2-purged 25 mL threeneck flask with 5 mL of additional ODE at 290 °C. Growth for 15 min yielded InP cores as determined by UV-vis and photoluminescence spectroscopy. The reaction temperature was reduced to 220 °C, and a solution of zinc stearate prepared by suspending 0.171 g (1.124 mmol) in 5 mL of ODE was injected into the reaction. After 15 min after temperature equilibration, TOP=Se (0.112 mL, 0.112 mmol) was added slowly over the course of 1 min, and the reaction equilibrated for 20 min. Next, TOP=S (1.011 mL, 1.011 mmol) was added slowly over the course of 5 min, and the reaction equilibrated for 15 min. The temperature was then set to 300 °C, and the photoluminescence was monitored until no further increases were measured (40 min following TOP=S injection). The reaction was cooled to room temperature, and the ODE was removed under vacuum distillation. The solid was suspended in toluene and centrifuged (7000 rpm for 10 min) to isolate the supernatant, which was then precipitated with acetonitrile. The precipitate was then resuspended in minimal toluene and purified by gel permeation chromatography.

Synthesis of Tetrahedral InP and InP/ZnS QDs. InP/ZnS core/shell QDs were prepared by following a procedure by Tessier et al. 80 Briefly, 100 mg (0.45 mmol) of indium(III) chloride and 300 mg (2.2 mmol) of zinc(II) chloride were mixed in 5.0 mL (15 mmol) of technical grade oleylamine in a 50 mL three-neck flask. The reaction mixture was degassed at 120 °C for an hour and then heated to 180 °C under N_2 . At 180 °C, 0.45 mL (1.6 mmol) of tris(diethylamino)-phosphine was swiftly injected. For tetrahedral InP QDs, quench reaction after 30 min.

For core/shell InP/ZnS, at 20 min, 1 mL of TOP-S (2.2 M) was dropwise injected. At 60 min, the temperature was increased from 180 to 200 °C. At 120 min, 1 g of Zn(stearate)₂ in 4 mL of octadecene (ODE) was dropwise injected, and the temperature was increased from 200 to 220 °C. At 150 min, 0.7 mL of TOP=S (2.2 M) was dropwise injected, and the temperature was increased from 220 to 240 °C. At 180 min, 0.5 g of Zn(stearate)₂ in 2 mL of ODE was dropwise injected, and the temperature was increased from 240 to 260 °C. At 210 min, the reaction was arrested and cooled to room temperature. Both InP and InP/ZnS were purified by repeated precipitation and resuspension in 2-propanol and toluene, respectively, four times. Indium phosphide tetrahedron-shaped quantum dots were obtained by quenching the reaction after 20 min of InP growth instead of adding TOP-S.

Synthesis of Cd_3P_2 QDs. The 3.5 nm Cd_3P_2 cores were synthesized based on a prior report. 81 Briefly, 0.692 g (3.0 mmol)

of $Cd(OAc)_2$ and 0.910 g (7.05 mmol) of octylamine were added to 8 mL of toluene in a 50 mL three-neck flask. This solution was heated 30 °C, and 2 mL of $(P(SiMe_3)_3)$ solution (0.5 M in toluene) was injected rapidly. The reaction temperature was maintained at 30 °C for 24 h before the solution was removed from heat, precipitated with ethanol, and resuspended in toluene five times.

Synthesis of Tetrapods with CdS Arms. Core/CdS tetrapod heterostructures were synthesized by using modifications of existing literature procedures. ^{17,82} Briefly, 2.65 g of TOPO (99%), 0.05175 g of CdO, 0.5 mL OA, and either 135 mg of ODPA (for thin arms) or 54 mg of ODPA (for thick arms) were degassed at 150 °C for 1.5 h in a 50 mL three-neck flask. The reaction mixture was heated to 350 $^{\circ}\text{C}$ under N2, and the reddish-brown solution turned colorless. Separately, a stock solution of TOP=S was made from 70 mg of sulfur with 6 mL of TOP (0.364 M). 0.6 mL of TOP=S was mixed with 2.5×10^{-9} mol of QDs as determined by the optical absorbance of the QD solution. Size and concentration quantification of QD cores have been reported previously for CdSe, 83 ZnTe, 72 InP, 84 and CIS. 7 Upon reaching the desired injection temperature of 350 °C, 1.8 mL of TOP was added, and the temperature was allowed to recover to 350 °C before the mixture of TOP=S and QDs was swiftly injected. Anisotropic CdS arms were grown at this temperature for 10 min. The heating mantle was removed, and the solution was cooled to room temperature. The core/CdS tetrapods were purified by repeated precipitation in methanol and redispersion in toluene five times.

Sample Characterization. UV-vis absorption spectra were obtained by using an Agilent Cary 5000 spectrophotometer, and fluorescence measurements were obtained on a Horiba Jobin Yvon FluoroMax-4 fluorescence spectrophotometer and an Edinburgh FLS 1000 fluorometer. Near-infrared photoluminescence was acquired on a home-built spectrometer by using amplitude-modulated excitation and phase-sensitive detection. Emission was separated with a monochromator and then detected by using a dual-band Si/InGaAs photodetector, and all traces were corrected for detector response. Samples were irradiated with a modulated (200 Hz) 365 nm LED or 550 nm LED by using appropriate long pass filters to remove scattered pump light prior to entrance into the monochromator. A PerkinElmer Optima 8300 inductively coupled plasma-optical emission spectrophotometer was used for elemental analysis. TEM images were obtained on an FEI Technai G2 F20 microscope. EDX data were typically obtained after plasma treating samples. Plasma treatment was performed on previously prepared TEM grids, sample side up, using H₂/O₂ in a 50:50 ratio for 4 min. Imaging was performed immediately afterward. Analysis of TEM images was performed using ImageJ software. Powder X-ray diffraction data were recorded on a Bruker D8 Discover instrument with the I μ S 2-D XRD system.

■ RESULTS AND DISCUSSION

Tetrapods were synthesized via hot injection of the seed QDs and sulfur precursor into a bath of *in situ* prepared cadmium precursor at 350 °C with a variable ratio of oleic and octadecylphosphonic acid (Figure 1). The aspect ratio of the

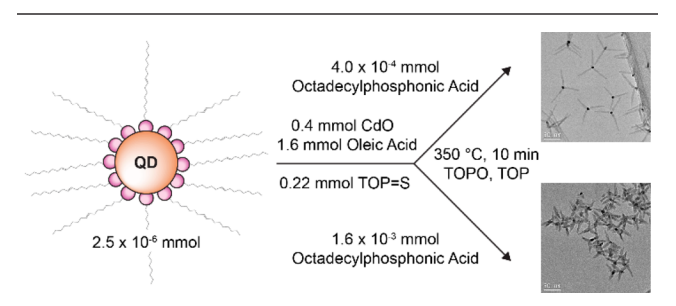


Figure 1. General reaction conditions for the synthesis of thick and thin arm tetrapods. TEM of example thick and thin arm tetrapods grown from ZnTe seeds.

arms was tuned by adjusting the ratio of octadecylphosphonic acid to oleic acid used to form the cadmium precursor—higher amounts of more strongly binding octadecylphosphonic acid give thinner arms as has been previously demonstrated in the literature. ¹⁷

Starting from 2.5×10^{-6} mmol of QDs (between 7.0×10^{-4} and 0.025 mmol total cations for 3 and 10 nm InP quantum dots, respectively, as a representative sample), 0.4 mmol of cadmium and 0.2 mmol of sulfur precursor are required for arm growth. Considering the orders of magnitude higher concentration of precursor compared to the seeds, we performed a set of control reactions to look for independent nucleation of CdS tetrapods under the reaction conditions. This is especially necessary given that cadmium sulfide is known to exhibit wurtzite—zinc blende polytypism. ⁵⁹ In the absence of seed QDs, CdS arm growth conditions gave rise to nanorods bearing one bulbous end (Figure 2). A minor

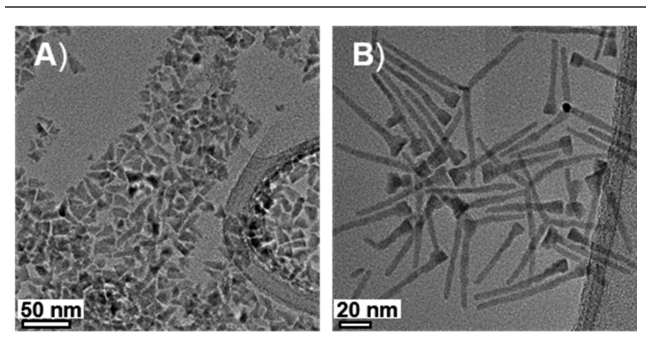


Figure 2. TEM images of CdS arms grown in the absence of nanocrystal seeds. Thick arm (A) and thin arm (B) morphology conditions. Measurements of particle dimensions are included in Table S1.

population of tetrapods was observed in the absence of seeds, representing <1% and <5% of the total observed nanostructures in the ensemble by TEM analysis for thick and thin arm morphology conditions, respectively. Additional ensemble images are shown in Figure S1 of the Supporting Information. Measurements of CdS arm length for all tetrapod samples (including the unseeded CdS arm control) are included in Table S1. Elemental analysis using ICP-OES gave a roughly 2:1 Cd:S ratio for both the thin and thick nanorod morphologies. Steady-state photoluminescence showed dominant trap emission (between 600 and 1000 nm) with a small component of band edge emission (~490 nm) as shown in Figure S2. These results demonstrate the need for QD seeds to facilitate tetrapod growth.

We next re-examined the synthesis of CdSe/CdS tetrapods to establish a baseline for tetrapod synthesis, purification, and analysis. ^{16,17,68} Notably, this work highlighted the challenge of probing the composition of tetrapod structures because, unlike core—shell systems where the core and shell components are often on the same order of magnitude by volume, tetrapod arms are typically multiple orders of magnitude greater in volume than the core. Thus, it was unsurprising that powder X-ray diffraction (XRD) analysis of conventional CdSe/CdS tetrapods gave features dominated by CdS, as shown in Figure S3. These observations are corroborated by previous reports of CdSe/CdS tetrapod systems. ¹⁶

Moving forward within the II–VI heterostructure family, we were interested in ZnTe/CdS tetrapods because the offset bulk band alignment is an attractive type II heterostructure and

because of our previous observations of facile zinc for cadmium cation exchange in related heterostructures. Beginning with 8 nm oblong ZnTe seeds (aspect ratio of 2), highly monodisperse tetrapods were obtained as shown in Figure 3.

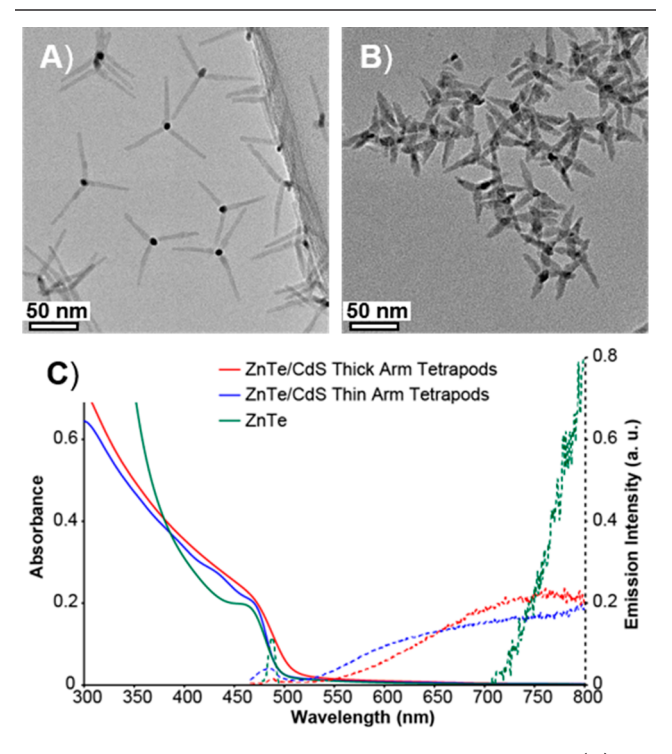


Figure 3. TEM images of ZnTe/CdS tetrapods with thick (A) and thin (B) arm morphologies along with the absorbance and emission of the ZnTe cores and ZnTe/CdS tetrapods (C). Measurements of arm dimensions are included in Table S1.

TEM images of ZnTe seeds are provided in Figure S4. Similar to a prior report documenting ZnTe/CdS tetrapod heterostructures, broad red-shifted optical features were observed, as can be seen in Figure 3. 64 This red-shifted luminescence was previously attributed to successful formation of the desired type II heterostructure; however, by ICP-OES analysis, we observed partial cation exchange in the final tetrapod products after a 10 min arm growth period. Starting from 1.1:1 Zn:Te cores, this ratio diminished to 1:5 and 1:3 in the thick and thin arm morphologies, respectively. Weak signals from zinc and tellurium in the core by EDX indicate that some ZnTe character may remain as shown in Figure S5. Taken together, optical and elemental characterizations suggest the formation of alloyed core Zn_{1-x}Cd_xTe/CdS heterostructures.

Similar to ZnTe, copper indium sulfide (CIS) also has a predicted type II or quasi-type II band alignment with CdS. ^{70,85–87} In addition, CIS nanocrystals have emerged as an alternative to cadmium- and lead-based materials due to their tunable photoluminescence across the visible and near-infrared spectrum, low toxicity, and large absorption cross section. ^{88–94} However, CIS has seen limited use in heterostructure development, likely due to its tetragonal crystal structure. ⁷⁰ This elongated lattice allows us to test the versatility of CdS arm growth by providing a distorted (111) plane as the surface for seeding wurtzite CdS arm growth. With moderate success, we synthesized tetrapods from 3 and 6 nm CIS cores. The larger 6 nm cores resulted in a greater yield of more uniform CIS/CdS tetrapod structures (Figure 4). This is

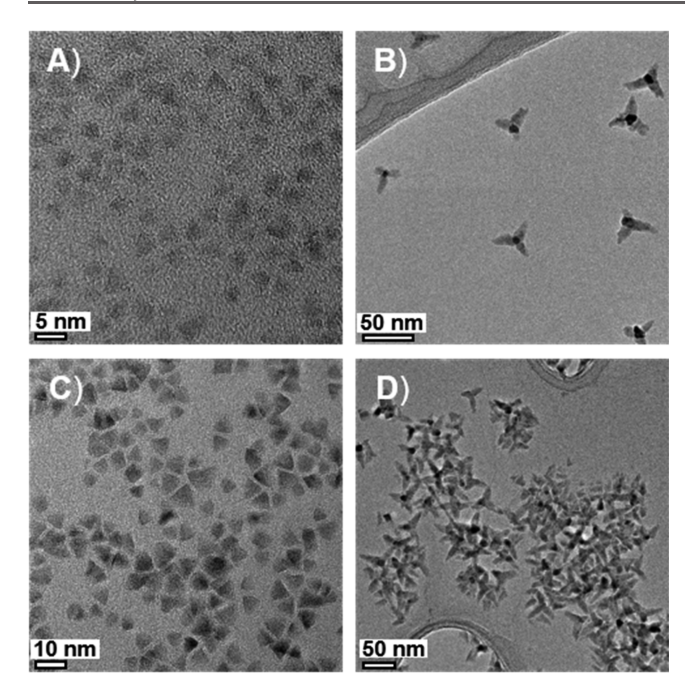


Figure 4. TEM images of CIS nanocrystals and CIS/CdS thick arm tetrapods: (A) 3 nm CIS, (B) CIS/CdS tetrapods from 3 nm CIS cores, (C) 6 nm CIS, and (D) CIS/CdS tetrapods from 6 nm CIS cores. Table S1 includes measurements of arm dimensions.

likely due to more well-defined and less strained (111) planes in the larger CIS nanocrystal seeds. Optical characterization for CIS seeded tetrapods and TEM of thin arm tetrapods is included in Figures S6 and S7. Cation exchange between cadmium and zinc for copper is known to occur in sulfide lattices. 15 Surprisingly, however, indium also appears to be mobile under our synthesis conditions. Elemental analysis of CIS/CdS tetrapods by ICP-OES showed no detectable levels of indium, suggesting that all indium from the core was removed by cation exchange during arm growth. The remaining copper content in both the thin and thick arm tetrapods assembled from both 3 and 6 nm CIS was 0.1% in a system that is 2:1 Cd:S. The starting 3 and 6 nm CIS cores were both slightly copper and cation rich with compositional ratios of 1.2:1.0:1.7 for Cu:In:S, similar to prior reports. 77,95 EDX of a single tetrapod shows weak signal from copper but no indium in the 6 nm CIS cores (Figure S8). Thus, both copper and indium are removed from the core via cation exchange. Both cation exchange and CdS arm growth begin rapidly upon addition of all precursors to the reaction vessel, suggesting that these processes occur concurrently. While CIS seeds arm growth, the core becomes primarily CdS in the resulting tetrapod. The photoluminescence spectra show emission from the tetrapods is dominated by trap emission, but complete suppression of any CdS band edge emission is also notable. The presence of copper has been reported to suppress band edge emission and give a highly red-shifted luminescence in CdSe, InP, and CIS quantum dots. 96-100 The intensity of broad trap emission from the CdS arm, however, dominates emission at energies above 650 nm as shown in Figures S6 and S7.

We next turned to phosphide lattices as scaffolds for tetrapod growth. III—V/II—VI heterostructure systems are highly sought after but significantly less studied than their II—VI/II—VI counterparts. Reports of incorporating InP into

anisotropic structures are uncommon due to its strong thermodynamic preference for the zinc blende crystal phase, with the wurtzite phase being only metastable.⁴⁹ Tetrapods were seeded by 3.0 nm zinc blende InP cores, as shown in Figure 5. A prior report noted decomposition of the InP core

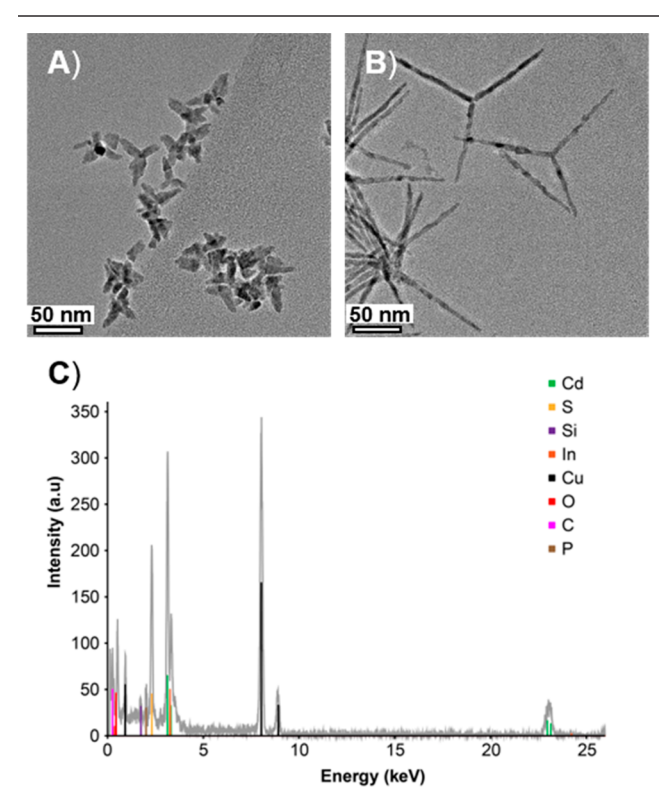


Figure 5. TEM images of InP/CdS tetrapods with thick (A) and thin (B) arm morphologies. (C) EDX of the InP/CdS tetrapods obtained by a point scan positioned at the tetrapod core. Analysis performed using copper grids. Measurements of arm dimensions are tabulated in Table S1.

under similar tetrapod growth conditions.⁷¹ Unsurprisingly, given this precedent, our InP cores did not retain their initial structure in the final tetrapods. Starting from 2:1 In:P cores, the final tetrapod heterostructures showed primarily cadmium and sulfur compared to only a small percentage of phosphorus (~3%) in the final tetrapod structure. However, phosphorus quantification is complicated by the use of phosphonate ligands during CdS arm growth. In seedless CdS growth, product structures typically contained 2-3% phosphorus. Indium was not observed by elemental analysis using ICP-OES within detectable limits, which may point to cation exchange whereby indium is removed and replaced with cadmium as seen previously.⁷⁴ Thus, while it is challenging to directly characterize the core of the tetrapod, these observations suggest the core of the final tetrapod is primarily cadmium phosphide in character. The optical properties of InP seeded tetrapods is shown in Figure S9. The optical properties are dominated by CdS without any optical transitions that can be contributed to the InP cores. Single-particle EDX evaluation of tetrapods showed a broadened signal in the spectral region associated with cadmium and indium, especially at the core (Figure 5). This, coupled with a relatively stronger signal from phosphorus, suggests that there may be minimal indium phosphide character remaining in the core component of the heterostructure.

Tetrahedral-shaped InP QDs were obtained by using tris(diethylamino)phosphine as the phosphorus precursor (Figure \$10). These faceted QDs retain a zinc blende lattice, and we postulated that the tetrahedral morphology could provide four well-defined facets for CdS growth. Tetrapods seeded from tetrahedral-shaped, amine-capped 3.3 nm InP were successfully synthesized with an average arm length of ~49 nm and width of ~4.7 nm (Figure 6). As expected, the

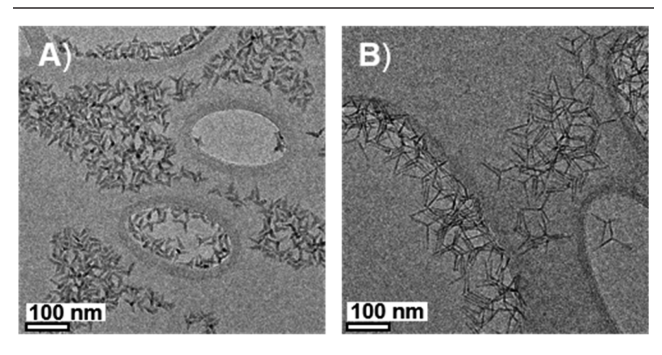


Figure 6. TEM images of InP/CdS tetrapods grown from tetrahedron-shaped InP nanocrystals showing thick (A) and thin (B) arm morphologies. Table S1 includes measurements of arm dimensions.

absorbance profile was dominated by CdS (Figure S11). The InP cores exhibited both band edge emission at 625 nm and broad trap emission between 700 and 1100 nm. After arm growth, there was no longer band edge emission from InP, despite the expected type I band alignment between InP and CdS, suggesting the core is no longer uniquely InP. By elemental analysis only ~0.02% indium relative to cadmium remained. On the basis of the dimensions of the core and arms, we would expect there to be ~2% indium relative to cadmium in the tetrapod. Thus, we propose that these tetrapods exhibit both cation exchange and tetrapod arm growth on similar time scales as was found in the earlier systems. Regardless of seed morphology, tetrapod arm growth and cation exchange within the core occur simultaneously to give tetrapods that are predominantly Cd₃P₂/CdS with small amounts of remaining indium in the core.

The same outcome was observed when starting from thinly shelled (~1 monolayer) InP/ZnSeS QDs with a 69% quantum yield. Once again, tetrapods were obtained, as can be seen in Figure S12 by TEM, but evaluation by ICP-OES reveals <0.02% indium, indicating cation exchange is unimpeded. The corresponding absorbance and fluorescence spectra associated with these samples are presented in Figure 7 and show the initially strong luminescence from the InP/ZnSeS core is no longer present.

To better understand the competing mechanisms of arm growth and cation exchange, InP cores with ~8 monolayers of ZnS were next used to obtain tetrapods. Using thicker shells offers two potential advantages: (i) preservation of the InP core by sacrificing the outer layers of zinc to cation exchange during arm growth and (ii) providing spectroscopic handle for characterization by elemental analysis and optical spectroscopy. The ZnS, if still intact, would give a type I heterostructure in the tetrapod core, making spatially indirect exciton recombination unfavorable. Thus, broad red-shifted optical signatures can be assigned to cation exchange yielding an indium—cadmium phosphide alloyed core rather than retaining the original InP/ZnS core—shell structure.

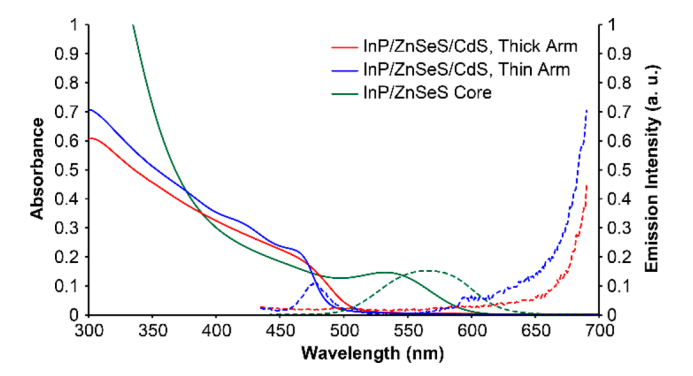


Figure 7. Absorbance and photoluminescence of InP/ZnSeS cores and InP/ZnSeS/CdS tetrapods with thick and thin CdS arm morphologies.

We successfully synthesized tetrapods starting from carboxylate-capped InP/ZnS (~6 nm) (Figure 8). Despite

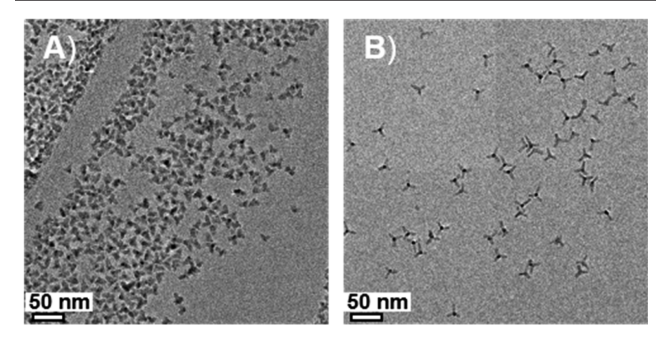


Figure 8. TEM images of InP/ZnS(thick)/CdS tetrapods with thick (A) and thin (B) arm morphologies. Measurements of arm dimensions are included in Table S1.

the shorter arms, the absorbance spectrum was still dominated by CdS (Figures S13 and S14). In contrast, the emission spectrum underwent a dramatic bathochromic shift and broadening. Thus, we can be confident that the original core/shell seed has undergone cation exchange during arm growth.

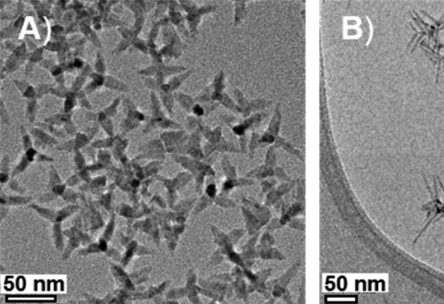
Quenching the reaction after 2 min gave triangular-pyramidshaped structures where arm growth was arrested prematurely (Figure S15). The CdS excitonic absorbance features were not yet fully defined, but the fluorescence spectrum had already shifted beyond 1100 nm (Figures S13 and S14). XRD of both the 2 and 10 min samples revealed only hexagonal CdS (Figure S16). Elemental analysis of these samples along with the starting InP/ZnS core showed that the ratio of indium to zinc remained relatively constant after 2 min of growth but decreased 10-fold after 10 min of tetrapod growth (Figure S17). This indicates that the thick ZnS shell temporarily serves as a protective layer to the core while seeding CdS over the first 2 min of arm growth. We propose that the resultant core is heavily alloyed with a gradient interface that grows into CdS arms. Cation exchange within the core is observed simultaneously with continued arm growth. The decreasing indiumto-zinc ratio between 2 and 10 min suggests that indium is more rapidly removed from the heterostructure as compared to zinc despite being encapsulated within the ZnS shell. The final location of zinc cations could not be determined, though zinc migration and induced disorder in phosphide and sulfide lattices remain a topic of interest. 101,102

Considering the observed cation exchange of cadmium for zinc, indium, and copper in our tetrapod systems, we believe that prior reports of tetrapods with these cations at the core also do not retain a well-defined structure. Despite excellent TEM evaluation and spectroscopic analysis that can be interpreted as heterostructure formation, we instead find that cation exchange is a dominant mechanism when these cores are subjected to CdS arm growth conditions. Cation exchange has been observed previously under similar conditions. 72,73,103 While cation exchange does not prevent tetrapod assembly, significant alloying is observed contrary to the conclusions in many prior reports. Red-shifting and broadening of the optical features of reported heterostructures (such as ZnTe/CdS) are typically attributed to spatially indirect emission of type II heterostructures between a core and a newly grown shell or arm. Spatially indirect emission with longer exciton lifetimes has been reported previously in nanoplatelet and core-shell type II and quasi-type II, II-IV nano-heterostructures. 28,104,105 In a previous report on InP/ZnS/CdS tetrapods, broadened emission and longer excitation lifetimes were observed and attributed to spatially indirect emission.⁷¹ However, broad, red-shifted optical features may also be a symptom of cation exchange. Cation exchange products have been observed to have broadened emission compared to the original quantum dot in InP quantum dots treated with cadmium and zinc. 106

Furthermore, exciton lifetime measurements may also be an inconclusive tool for evaluating the difference between heterostructure and cation diffusion nanostructures. In a (Zn,Cd)Se system by de Mello Donega and co-workers, increasing the temperature resulted in a transition from coreshell to gradient alloy to homogeneous alloy nanostructures. Exciton lifetime decreased across this transition. Interestingly, the emission for the cation exchange products does not broaden noticeably. However, this is most likely a function of this particular system that is highly monodisperse and has likely reached thermodynamic equilibrium. Because both cation exchange and spatially indirect band gap emission can have broad PL, there is not a simple and obvious way to see the difference.

Another important optical feature to keep in mind is CdS trap emission. Reported red-shifted emission features may actually be trap emission from the CdS arms. This has been explored in depth in CdS systems, and the presence of this strong emissive feature is seen in all of our tetrapod structures. Despite the increased trap emission, CdS band edge emission is suppressed in seeded architectures. Considering that optical properties alone are inadequate for unambiguous characterization of heterostructures and cation exchange systems, further compositional characterization should be a requirement. In addition to elemental analysis techniques such as ICP-OES and ICP-MS, EXAFS also provides valuable insights into the elemental composition of these types of systems. 101,103,113

One system where this general approach to heterostructure development was successful while retaining clean interfaces between the core and arm components is Cd_3P_2/CdS tetrapods. In this system, ~ 3.5 nm Cd_3P_2 QDs were used to seed thick and thin arm tetrapods (Figure S18). Cubic Cd_3P_2 QDs, prepared using tris(trimethylsilyl)phosphine gave tetrapods within 10 min of precursor and seed injection. As can be seen in Figure 9, TEM imaging confirmed the assembly of tetrapod architectures with both arm motifs.



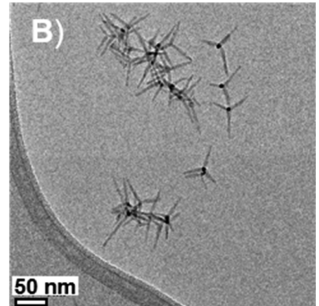


Figure 9. TEM images of $Cd_3P_2(3.5 \text{ nm})/CdS$ tetrapods with thick (A) and thin (B) arm morphologies. Measurements of arm dimensions are included in Table S1.

Evaluation of the optical properties of Cd_3P_2/CdS tetrapods confirms electronic communication between the arm and core components. Absorbance and emission spectra of both the Cd_3P_2 core (Figure S19) and Cd_3P_2/CdS tetrapods (Figure 10

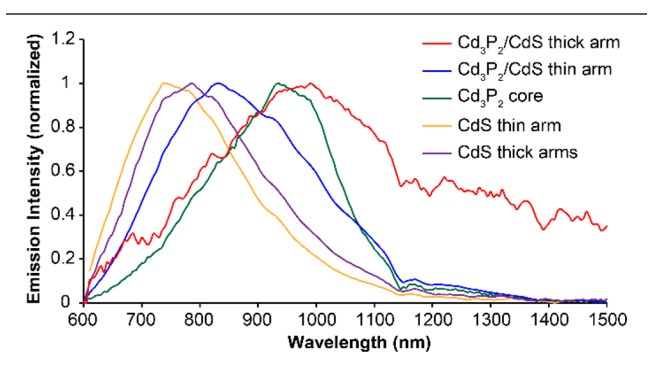


Figure 10. Emission of Cd_3P_2 nanocrystals, Cd_3P_2/CdS tetrapods, and CdS arms with thick and thin arm morphologies. Strong emission features from the Cd_3P_2 core are observed at 1100 nm (1.13 eV) prior to tetrapod assembly. This emission shifts up to 82 meV when incorporated into tetrapods.

and Figure S20) are located in the Supporting Information. Cd₂P₂/CdS tetrapods have a broad, NIR emission characteristic of Cd₃P₂ between 900 and 1200 nm and suppression of band edge emission from CdS when illuminated with 365 nm light. While the emission peak maximum is relatively unchanged between the Cd₃P₂ core and the thick arm tetrapods, the emission from the thin arm tetrapods undergoes a hypsochromic shift. A similar pattern has been observed in CdSe/CdS tetrapods. 17 Two explanations for this phenomenon have been proposed previously: strong quantum confinement remains present along the short axis perpendicular to the arm length, and electron wave function leakage does not extend beyond a certain arm length in quasi-type II heterostructures.¹⁷ However, the hypsochromic shift may also be due to etching of the seed's surface prior to arm growth and the increased, asymmetrical strain induced by the thin arms relative to their thick arm counterparts.

The emission between 600 and 900 nm is attributed to trap emission from the CdS arms and is in line with prior reports. Because CdS has a high molar extinction coefficient and accounts for >99% of the tetrapod's volume, all excitation at 365 nm is attributed to absorbance within the arms. The $\rm Cd_3P_2$ cores account for <1% of the tetrapod's volume and are undetectable by XRD. Furthermore, under illumination beyond the absorbance edge of CdS with a green

LED (550 nm), no fluorescence was detected for Cd_3P_2/CdS tetrapods or Cd_3P_2 cores. This indicates strong electronic communication between the core and arms in this type I heterostructure configuration where the CdS arms absorb and emission arises from the Cd_3P_2 core.

To rule out all interparticle energy and charge transfer processes, the emissive properties of mixtures of cores and CdS arms were evaluated. Figure S21 depicts the emission spectra of solutions of Cd_3P_2 cores mixed with independent CdS arms (thick and thin morphologies) in 1:1 optical density ratio at 365 nm along with spectra of the Cd_3P_2 core and CdS arm emission spectra. The emission traces of each mixture of arms and cores closely match the sum of the emission spectra for the arms and cores independently of one another for both the thin and thick arm morphologies. This indicates that NIR emission observed from the Cd_3P_2/CdS tetrapods arises from CdS arm absorption and Cd_3P_2 emission without contributions from interparticle charge or energy transfer processes.

CONCLUSIONS

A seeded growth approach was used to obtain tetrapod nanostructures. Essentially almost any seed with accessible (111) planes could be used as a scaffold for tetrapod arm growth. This approach extends beyond cubic cores to those with tetragonal lattices that have distorted (111) planes, such as CIS. However, cation exchange accompanies the process of arm growth in many systems, precluding access to clean interfaces and desirable heterostructure band alignments. This work demonstrates that cation exchange and ion migration should always be a consideration when designing and characterizing heterostructures since both processes are often favorable under the same reaction conditions as crystal growth, and are not mutually exclusive. Ultimately, we use our general principles of arm growth to synthesize NIR emissive Cd₃P₂/ CdS tetrapod heterostructures. Identifying conditions to suppress ion migration while still enabling wurtzite structure arm growth would be a productive next step in the synthesis of anisotropic nanoscale heterostructures.

ASSOCIATED CONTENT

Supporting Information

The Supporting Information is available free of charge at https://pubs.acs.org/doi/10.1021/acs.chemmater.0c01407.

Table containing tetrapod arm dimensions as determined by TEM analysis (Table S1); additional supporting data including TEM images, steady-state optical spectra (UV–vis, PL), powder X-ray diffraction, EDX, and ICP analysis (Figures S1–S21) (PDF)

AUTHOR INFORMATION

Corresponding Author

Brandi M. Cossairt — Department of Chemistry, University of Washington, Seattle, Washington 98195-1700, United States; orcid.org/0000-0002-9891-3259; Email: cossairt@uw.edu

Authors

Michael J. Enright — Department of Chemistry, University of Washington, Seattle, Washington 98195-1700, United States Florence Y. Dou — Department of Chemistry, University of Washington, Seattle, Washington 98195-1700, United States Shenwei Wu — Department of Chemistry, University of Washington, Seattle, Washington 98195-1700, United States

Emily J. Rabe — Department of Chemistry, University of Washington, Seattle, Washington 98195-1700, United States; orcid.org/0000-0002-9397-049X

Madison Monahan — Department of Chemistry, University of Washington, Seattle, Washington 98195-1700, United States

Max R. Friedfeld — Department of Chemistry, University of Washington, Seattle, Washington 98195-1700, United States

Cody W. Schlenker — Department of Chemistry, University of Washington, Seattle, Washington 98195-1700, United States;

orcid.org/0000-0003-3103-402X

Complete contact information is available at: https://pubs.acs.org/10.1021/acs.chemmater.0c01407

Notes

The authors declare no competing financial interest.

ACKNOWLEDGMENTS

B.C., M.E., and F.D. thank generous support from the National Science Foundation EAGER program under Grant CHE-1836500. F.D. was also supported by a follow-up grant from the National Science Foundation under Grant MPS-1936100. This work stems from a collaboration with Professor Arka Majumdar, whom we thank for productive discussions. Part of this work was conducted at the Molecular Analysis Facility, a National Nanotechnology Coordinated Infrastructure site at the University of Washington, which is supported in part by the National Science Foundation (Grant NNCI-1542101), the University of Washington, the Molecular Engineering & Sciences Institute, and the Clean Energy Institute. Part of this work made use of instrumentation supported by the University of Washington Molecular Engineering Materials Center (MEM-C), a Materials Research Science and Engineering Center (MRSEC) sponsored by the National Science Foundation under Grant DMR-1719797.

REFERENCES

- (1) Shi, W.; Hughes, R. W.; Denholme, S. J.; Gregory, D. H. Synthesis design strategies to anisotropic chalcogenide nanostructures. *CrystEngComm* **2010**, *12*, 641–659.
- (2) Burda, C.; Chen, X.; Narayanan, R.; El-Sayed, M. A. Chemistry and Properties of Nanocrystals of Different Shapes. *Chem. Rev.* **2005**, 105, 1025–1102.
- (3) Sajanlal, P. R.; Sreeprasad, T. S.; Samal, A. K.; Pradeep, T. Anisotropic nanomaterials: structure, growth, assembly, and functions. *Nano Rev.* **2011**, *2*, 5883.
- (4) Peng, X.; Manna, L.; Yang, W.; Wickham, J.; Scher, E.; Kadavanich, A.; Alivisatos, A. P. Shape control of CdSe nanocrystals. *Nature* **2000**, *404*, 59–61.
- (5) Peng, Z. A.; Peng, X. Nearly Monodisperse and Shape-Controlled CdSe Nanocrystals via Alternative Routes: Nucleation and Growth. *J. Am. Chem. Soc.* **2002**, *124*, 3343–3353.
- (6) Enright, M. J.; Cossairt, B. M. Synthesis of tailor-made colloidal semiconductor heterostructures. *Chem. Commun.* **2018**, *54*, 7109–7122
- (7) Peng, X. Mechanisms for the Shape-Control and Shape-Evolution of Colloidal Semiconductor Nanocrystals. *Adv. Mater.* **2003**, *15*, 459–463.
- (8) Talapin, D. V.; Rogach, A. L.; Kornowski, A.; Haase, M.; Weller, H. Highly Luminescent Monodisperse CdSe and CdSe/ZnS Nanocrystals Synthesized in a Hexadecylamine-Trioctylphosphine Oxide-Trioctylphospine Mixture. *Nano Lett.* **2001**, *1*, 207–211.
- (9) Murray, C. B.; Norris, D. J.; Bawendi, M. G. Synthesis and characterization of nearly monodisperse CdE (E = sulfur, selenium, tellurium) semiconductor nanocrystallites. *J. Am. Chem. Soc.* **1993**, *115*, 8706–8715.

- (10) Peng, X.; Wickham, J.; Alivisatos, A. P. Kinetics of II-VI and III-V Colloidal Semiconductor Nanocrystal Growth: "Focusing" of Size Distributions. *J. Am. Chem. Soc.* **1998**, *120*, 5343–5344.
- (11) Hu, J.; Li, L.-S.; Yang, W.; Manna, L.; Wang, L.-W.; Alivisatos, A. P. Linearly Polarized Emission from Colloidal Semiconductor Quantum Rods. *Science* **2001**, *292*, 2060–2063.
- (12) Tsivion, D.; Schvartzman, M.; Popovitz-Biro, R.; von Huth, P.; Joselevich, E. Guided Growth of Millimeter-Long Horizontal Nanowires with Controlled Orientations. *Science* **2011**, 333, 1003–1007
- (13) Manna, L.; Scher, E. C.; Alivisatos, A. P. Synthesis of Soluble and Processable Rod-, Arrow-, Teardrop-, and Tetrapod-Shaped CdSe Nanocrystals. *J. Am. Chem. Soc.* **2000**, *122*, 12700–12706.
- (14) Enright, M. J.; Sarsito, H.; Cossairt, B. M. Kinetically controlled assembly of cadmium chalcogenide nanorods and nanorod heterostructures. *Mater. Chem. Front.* **2018**, *2*, 1296–1305.
- (15) Fenton, J. L.; Steimle, B. C.; Schaak, R. E. Tunable intraparticle frameworks for creating complex heterostructured nanoparticle libraries. *Science* **2018**, *360*, 513–517.
- (16) Talapin, D. V.; Nelson, J. H.; Shevchenko, E. V.; Aloni, S.; Sadtler, B.; Alivisatos, A. P. Seeded Growth of Highly Luminescent CdSe/CdS Nanoheterostructures with Rod and Tetrapod Morphologies. *Nano Lett.* **2007**, *7*, 2951–2959.
- (17) Mishra, N.; Wu, W.-Y.; Srinivasan, B. M.; Hariharaputran, R.; Zhang, Y.-W.; Chan, Y. Continuous Shape Tuning of Nanotetrapods: Toward Shape-Mediated Self-Assembly. *Chem. Mater.* **2016**, 28, 1187–1195.
- (18) Boschker, H.; Mannhart, J. Quantum-Matter Heterostructures. Annu. Rev. Condens. Matter Phys. 2017, 8, 145–164.
- (19) Conca, E.; Aresti, M.; Saba, M.; Casula, M. F.; Quochi, F.; Mula, G.; Loche, D.; Kim, M. R.; Manna, L.; Corrias, A.; Mura, A.; Bongiovanni, G. Charge separation in Pt-decorated CdSe@CdS octapod nanocrystals. *Nanoscale* **2014**, *6*, 2238–2243.
- (20) Ghosh Chaudhuri, R.; Paria, S. Core/Shell Nanoparticles: Classes, Properties, Synthesis Mechanisms, Characterization, and Applications. *Chem. Rev.* **2012**, *112*, 2373–2433.
- (21) Gawande, M. B.; Goswami, A.; Asefa, T.; Guo, H.; Biradar, A. V.; Peng, D.-L.; Zboril, R.; Varma, R. S. Core–shell nanoparticles: synthesis and applications in catalysis and electrocatalysis. *Chem. Soc. Rev.* **2015**, *44*, 7540–7590.
- (22) Kortan, A. R.; Hull, R.; Opila, R. L.; Bawendi, M. G.; Steigerwald, M. L.; Carroll, P. J.; Brus, L. E. Nucleation and Growth of CdSe on ZnS Quantum Crystallite Seeds, and Vice Versa, in Inverse Micelle Media. J. Am. Chem. Soc. 1990, 112, 1327–1332.
- (23) Hines, M. A.; Guyot-Sionnest, P. Synthesis and Characterization of Strongly Luminescing ZnS-Capped CdSe Nanocrystals. *J. Phys. Chem.* **1996**, *100*, 468–471.
- (24) Dabbousi, B. O.; Rodriguez-Viejo, J.; Mikulec, F. V.; Heine, J. R.; Mattoussi, H.; Ober, R.; Jensen, K. F.; Bawendi, M. G. (CdSe)ZnS Core-Shell Quantum Dots: Synthesis and Characterization of a Size Series of Highly Luminescent Nanocrystallites. *J. Phys. Chem. B* **1997**, *101*, 9463–9475.
- (25) Nandan, Y.; Mehata, M. S. Wavefunction Engineering of Type-I/Type-II Excitons of CdSe/CdS Core-Shell Quantum Dots. *Sci. Rep.* **2019**, *9*, 2.
- (26) Jiao, S.; Shen, Q.; Mora-Seró, I.; Wang, J.; Pan, Z.; Zhao, K.; Kuga, Y.; Zhong, X.; Bisquert, J. Band Engineering in Core/Shell ZnTe/CdSe for Photovoltage and Efficiency Enhancement in Exciplex Quantum Dot Sensitized Solar Cells. ACS Nano 2015, 9, 908–915.
- (27) Wang, J.; Mora-Seró, I.; Pan, Z.; Zhao, K.; Zhang, H.; Feng, Y.; Yang, G.; Zhong, X.; Bisquert, J. Core/Shell Colloidal Quantum Dot Exciplex States for the Development of Highly Efficient Quantum-Dot-Sensitized Solar Cells. J. Am. Chem. Soc. 2013, 135, 15913—15922.
- (28) Kim, S.; Fisher, B.; Eisler, H.-J.; Bawendi, M. Type-II Quantum Dots: CdTe/CdSe(Core/Shell) and CdSe/ZnTe(Core/Shell) Heterostructures. *J. Am. Chem. Soc.* **2003**, *125*, 11466–11467.
- (29) Zhong, H.; Zhou, Y.; Yang, Y.; Yang, C.; Li, Y. Synthesis of Type II CdTe-CdSe Nanocrystal Heterostructured Multiple-

- Branched Rods and Their Photovoltaic Applications. *J. Phys. Chem.* C 2007, 111, 6538-6543.
- (30) Scholes, G. D.; Jones, M.; Kumar, S. Energetics of Photoinduced Electron-Transfer Reactions Decided by Quantum Confinement. J. Phys. Chem. C 2007, 111, 13777-13785.
- (31) Zhu, H.; Song, N.; Lian, T. Wave Function Engineering for Ultrafast Charge Separation and Slow Charge Recombination in Type II Core/Shell Quantum Dots. *J. Am. Chem. Soc.* **2011**, *133*, 8762–8771.
- (32) Lo, S. S.; Mirkovic, T.; Chuang, C.-H.; Burda, C.; Scholes, G. D. Emergent Properties Resulting from Type-II Band Alignment in Semiconductor Nanoheterostructures. *Adv. Mater.* **2011**, *23*, 180–197.
- (33) Mekis, I.; Talapin, D. V.; Kornowski, A.; Haase, M.; Weller, H. One-Pot Synthesis of Highly Luminescent CdSe/CdS Core-Shell Nanocrystals via Organometallic and "Greener" Chemical Approaches. J. Phys. Chem. B 2003, 107, 7454–7462.
- (34) Peng, X.; Schlamp, M. C.; Kadavanich, A. V.; Alivisatos, A. P. Epitaxial Growth of Highly Luminescent CdSe/CdS Core/Shell Nanocrystals with Photostability and Electronic Accessibility. *J. Am. Chem. Soc.* **1997**, *119*, 7019–7029.
- (35) Cragg, G. E.; Efros, A. L. Suppression of Auger Processes in Confined Structures. *Nano Lett.* **2010**, *10*, 313–317.
- (36) Saha, A.; Chellappan, K. V.; Narayan, K. S.; Ghatak, J.; Datta, R.; Viswanatha, R. Near-Unity Quantum Yield in Semiconducting Nanostructures: Structural Understanding Leading to Energy Efficient Applications. *J. Phys. Chem. Lett.* **2013**, *4*, 3544–3549.
- (37) Chen, Y.; Vela, J.; Htoon, H.; Casson, J. L.; Werder, D. J.; Bussian, D. A.; Klimov, V. I.; Hollingsworth, J. A. Giant" Multishell CdSe Nanocrystal Quantum Dots with Suppressed Blinking. *J. Am. Chem. Soc.* **2008**, 130, 5026–5027.
- (38) Pal, B. N.; Ghosh, Y.; Brovelli, S.; Laocharoensuk, R.; Klimov, V. I.; Hollingsworth, J. A.; Htoon, H. 'Giant' CdSe/CdS Core/Shell Nanocrystal Quantum Dots As Efficient Electroluminescent Materials: Strong Influence of Shell Thickness on Light-Emitting Diode Performance. *Nano Lett.* **2012**, *12*, 331–336.
- (39) Purcell-Milton, F.; Visheratina, A. K.; Kuznetsova, V. A.; Ryan, A.; Orlova, A. O.; Gun'ko, Y. K. Impact of Shell Thickness on Photoluminescence and Optical Activity in Chiral CdSe/CdS Core/Shell Quantum Dots. *ACS Nano* **2017**, *11*, 9207–9214.
- (40) Jiang, Z.-J.; Kelley, D. F. Effects of Inhomogeneous Shell Thickness in the Charge Transfer Dynamics of ZnTe/CdSe Nanocrystals. *J. Phys. Chem. C* **2012**, *116*, 12958–12968.
- (41) Kong, D.; Jia, Y.; Ren, Y.; Xie, Z.; Wu, K.; Lian, T. Shell-Thickness-Dependent Biexciton Lifetime in Type I and Quasi-Type II CdSe@CdS Core/Shell Quantum Dots. *J. Phys. Chem. C* **2018**, *122*, 14091–14098.
- (42) Hines, D. A.; Becker, M. A.; Kamat, P. V. Photoinduced Surface Oxidation and Its Effect on the Exciton Dynamics of CdSe Quantum Dots. *J. Phys. Chem. C* **2012**, *116*, 13452–13457.
- (43) Chappell, H. E.; Hughes, B. K.; Beard, M. C.; Nozik, A. J.; Johnson, J. C. Emission Quenching in PbSe Quantum Dot Arrays by Short-Term Air Exposure. *J. Phys. Chem. Lett.* **2011**, *2*, 889–893.
- (44) Myung, N.; Bae, Y.; Bard, A. J. Enhancement of the Photoluminescence of CdSe Nanocrystals Dispersed in CHCl₃ by Oxygen Passivation of Surface States. *Nano Lett.* **2003**, *3*, 747–749.
- (45) Zhu, H.; Song, N.; Lv, H.; Hill, C. L.; Lian, T. Near Unity Quantum Yield of Light-Driven Redox Mediator Reduction and Efficient H2 Generation Using Colloidal Nanorod Heterostructures. *J. Am. Chem. Soc.* **2012**, *134*, 11701–11708.
- (46) Amirav, L.; Alivisatos, A. P. Photocatalytic Hydrogen Production with Tunable Nanorod Heterostructures. *J. Phys. Chem. Lett.* **2010**, *1*, 1051–1054.
- (47) Kim, D.; Lee, Y. K.; Lee, D.; Kim, W. D.; Bae, W. K.; Lee, D. C. Colloidal Dual-Diameter and Core-Position-Controlled Core/Shell Cadmium Chalcogenide Nanorods. *ACS Nano* **2017**, *11*, 12461–12472.
- (48) Wu, K.; Hill, L. J.; Chen, J.; McBride, J. R.; Pavlopolous, N. G.; Richey, N. E.; Pyun, J.; Lian, T. Universal Length Dependence of

- Rod-to-Seed Exciton Localization Efficiency in Type I and Quasi-Type II CdSe@CdS Nanorods. ACS Nano 2015, 9, 4591–4599.
- (49) De Trizio, L.; Gaspari, R.; Bertoni, G.; Kriegel, I.; Moretti, L.; Scotognella, F.; Maserati, L.; Zhang, Y.; Messina, G. C.; Prato, M.; Marras, S.; Cavalli, A.; Manna, L. Cu3-xP Nanocrystals as a Material Platform for Near-Infrared Plasmonics and Cation Exchange Reactions. *Chem. Mater.* 2015, 27, 1120–1128.
- (50) De Luca, M.; Zilli, A.; Fonseka, H. A.; Mokkapati, S.; Miriametro, A.; Tan, H. H.; Smith, L. M.; Jagadish, C.; Capizzi, M.; Polimeni, A. Polarized Light Absorption in Wurtzite InP Nanowire Ensembles. *Nano Lett.* **2015**, *15*, 998–1005.
- (51) De, A.; Pryor, C. E. Predicted band structures of III-V semiconductors in the wurtzite phase. *Phys. Rev. B: Condens. Matter Mater. Phys.* **2010**, *81*, 155210.
- (52) Dacal, L. C. O.; Cantarero, A. Ab initio electronic band structure calculation of InP in the wurtzite phase. *Solid State Commun.* **2011**, *151*, 781–784.
- (53) Murayama, M.; Nakayama, T. Chemical trend of band offsets at wurtzite/zinc-blende heterocrystalline semiconductor interfaces. *Phys. Rev. B: Condens. Matter Mater. Phys.* **1994**, 49, 4710–4724.
- (54) Steimle, B. C.; Fenton, J. L.; Schaak, R. E. Rational construction of a scalable heterostructured nanorod megalibrary. *Science* **2020**, *367*, 418–424.
- (55) Mohamed, M. B.; Tonti, D.; Al-Salman, A.; Chemseddine, A.; Chergui, M. Synthesis of High Quality Zinc Blende CdSe Nanocrystals. *J. Phys. Chem. B* **2005**, *109*, 10533–10537.
- (56) Lincheneau, C.; Amelia, M.; Oszajca, M.; Boccia, A.; D'Orazi, F.; Madrigale, M.; Zanoni, R.; Mazzaro, R.; Ortolani, L.; Morandi, V.; Silvi, S.; Szaciłowski, K.; Credi, A. Synthesis and properties of ZnTe and ZnTe/ZnS core/shell semiconductor nanocrystals. *J. Mater. Chem. C* 2014, 2, 2877–2886.
- (57) Micic, O. I.; Curtis, C. J.; Jones, K. M.; Sprague, J. R.; Nozik, A. J. Synthesis and Characterization of InP Quantum Dots. *J. Phys. Chem.* **1994**, *98*, 4966–4969.
- (58) Li, L.-S.; Hu, J.; Yang, W.; Alivisatos, A. P. Band Gap Variation of Size- and Shape-Controlled Colloidal CdSe Quantum Rods. *Nano Lett.* **2001**, *1*, 349–351.
- (59) Manna, L.; Milliron, D. J.; Meisel, A.; Scher, E. C.; Alivisatos, A. P. Controlled growth of tetrapod-branched inorganic nanocrystals. *Nat. Mater.* **2003**, *2*, 382–385.
- (60) Mishra, N.; Vasavi Dutt, V. G.; Arciniegas, M. P. Recent Progress on Metal Chalcogenide Semiconductor Tetrapod-Shaped Colloidal Nanocrystals and their Applications in Optoelectronics. *Chem. Mater.* **2019**, *31*, 9216–9242.
- (61) Carbone, L.; Kudera, S.; Carlino, E.; Parak, W. J.; Giannini, C.; Cingolani, R.; Manna, L. Multiple Wurtzite Twinning in CdTe Nanocrystals Induced by Methylphosphonic Acid. *J. Am. Chem. Soc.* **2006**, *128*, 748–755.
- (62) Yeh, C.-Y.; Lu, Z. W.; Froyen, S.; Zunger, A. Zinc-blende-wurtzite polytypism in semiconductors. *Phys. Rev. B: Condens. Matter Mater. Phys.* **1992**, *46*, 10086–10097.
- (63) Fiore, A.; Mastria, R.; Lupo, M. G.; Lanzani, G.; Giannini, C.; Carlino, E.; Morello, G.; De Giorgi, M.; Li, Y.; Cingolani, R.; Manna, L. Tetrapod-Shaped Colloidal Nanocrystals of II-VI Semiconductors Prepared by Seeded Growth. *J. Am. Chem. Soc.* **2009**, *131*, 2274–2282.
- (64) Xie, R.; Kolb, U.; Basché, T. Design and Synthesis of Colloidal Nanocrystal Heterostructures with Tetrapod Morphology. *Small* **2006**, 2, 1454–1457.
- (65) Pavlopoulos, N. G.; Dubose, J. T.; Liu, Y.; Huang, X.; Pinna, N.; Willinger, M.-G.; Lian, T.; Char, K.; Pyun, J. Type I vs. quasi-type II modulation in CdSe@CdS tetrapods: ramifications for noble metal tipping. *CrystEngComm* **2017**, *19*, 6443–6453.
- (66) Sitt, A.; Sala, F. D.; Menagen, G.; Banin, U. Multiexciton Engineering in Seeded Core/Shell Nanorods: Transfer from Type-I to Quasi-type-II Regimes. *Nano Lett.* **2009**, *9*, 3470–3476.
- (67) Kelestemur, Y.; Cihan, A. F.; Guzelturk, B.; Demir, H. V. Typetunable amplified spontaneous emission from core-seeded CdSe/CdS

- nanorods controlled by exciton-exciton interaction. *Nanoscale* **2014**, 6, 8509-8514.
- (68) Mishra, N.; Orfield, N. J.; Wang, F.; Hu, Z.; Krishnamurthy, S.; Malko, A. V.; Casson, J. L.; Htoon, H.; Sykora, M.; Hollingsworth, J. A. Using shape to turn off blinking for two-colour multiexciton emission in CdSe/CdS tetrapods. *Nat. Commun.* **2017**, *8*, 15083.
- (69) Pang, Q.; Zhao, L.; Cai, Y.; Nguyen, D. P.; Regnault, N.; Wang, N.; Yang, S.; Ge, W.; Ferreira, R.; Bastard, G.; Wang, J. CdSe Nanotetrapods: Controllable Synthesis, Structure Analysis, and Electronic and Optical Properties. *Chem. Mater.* **2005**, *17*, 5263–5267.
- (70) Kim, B.; Kim, K.; Kwon, Y.; Lee, W.; Shin, W. H.; Kim, S.; Bang, J. CuInS2/CdS-Heterostructured Nanotetrapods by Seeded Growth and Their Photovoltaic Properties. *ACS Appl. Nano Mater.* **2018**, *1*, 2449–2454.
- (71) Wu, W.-Y.; Li, M.; Lian, J.; Wu, X.; Yeow, E. K. L.; Jhon, M. H.; Chan, Y. Efficient Color-Tunable Multiexcitonic Dual Wavelength Emission from Type II Semiconductor Tetrapods. *ACS Nano* **2014**, *8*, 9349–9357.
- (72) Enright, M. J.; Sarsito, H.; Cossairt, B. M. Quantifying Cation Exchange of Cd2+ in ZnTe: A Challenge for Accessing Type II Heterostructures. *Chem. Mater.* **2017**, *29*, 666–672.
- (73) Groeneveld, E.; Witteman, L.; Lefferts, M.; Ke, X.; Bals, S.; Van Tendeloo, G.; de Mello Donega, C. Tailoring ZnSe–CdSe Colloidal Quantum Dots via Cation Exchange: From Core/Shell to Alloy Nanocrystals. *ACS Nano* **2013**, *7*, 7913–7930.
- (74) Stein, J. L.; Steimle, M. I.; Terban, M. W.; Petrone, A.; Billinge, S. J. L.; Li, X.; Cossairt, B. M. Cation Exchange Induced Transformation of InP Magic-Sized Clusters. *Chem. Mater.* **2017**, 29, 7984–7992.
- (75) Gary, D. C.; Cossairt, B. M. Role of Acid in Precursor Conversion During InP Quantum Dot Synthesis. *Chem. Mater.* **2013**, 25, 2463–2469.
- (76) Enright, M. J.; Gilbert-Bass, K.; Sarsito, H.; Cossairt, B. M. Photolytic C-O Bond Cleavage with Quantum Dots. *Chem. Mater.* **2019**, *31*, 2677–2682.
- (77) Booth, M.; Brown, A. P.; Evans, S. D.; Critchley, K. Determining the Concentration of CuInS2 Quantum Dots from the Size-Dependent Molar Extinction Coefficient. *Chem. Mater.* **2012**, *24*, 2064–2070.
- (78) Gary, D. C.; Terban, M. W.; Billinge, S. J. L.; Cossairt, B. M. Two-Step Nucleation and Growth of InP Quantum Dots via Magic-Sized Cluster Intermediates. *Chem. Mater.* **2015**, *27*, 1432–1441.
- (79) Friedfeld, M. R.; Stein, J. L.; Johnson, D. A.; Park, N.; Henry, N. A.; Enright, M. J.; Mocatta, D.; Cossairt, B. M. Effects of Zn2+ and Ga3+ doping on the quantum yield of cluster-derived InP quantum dots. *J. Chem. Phys.* **2019**, *151*, 194702.
- (80) Tessier, M. D.; Dupont, D.; De Nolf, K.; De Roo, J.; Hens, Z. Economic and Size-Tunable Synthesis of InP/ZnE (E = S, Se) Colloidal Quantum Dots. *Chem. Mater.* **2015**, 27, 4893–4898.
- (81) Ojo, W.-S.; Xu, S.; Delpech, F.; Nayral, C.; Chaudret, B. Room-Temperature Synthesis of Air-Stable and Size-Tunable Luminescent ZnS-Coated Cd3P2 Nanocrystals with High Quantum Yields. *Angew. Chem., Int. Ed.* **2012**, *51*, 738–741.
- (82) Mishra, N.; Lian, J.; Chakrabortty, S.; Lin, M.; Chan, Y. Unusual Selectivity of Metal Deposition on Tapered Semiconductor Nanostructures. *Chem. Mater.* **2012**, *24*, 2040–2046.
- (83) Jasieniak, J.; Smith, L.; van Embden, J.; Mulvaney, P.; Califano, M. Re-examination of the Size-Dependent Absorption Properties of CdSe Quantum Dots. *J. Phys. Chem. C* **2009**, *113*, 19468–19474.
- (84) Xie, L.; Shen, Y.; Franke, D.; Sebastián, V.; Bawendi, M. G.; Jensen, K. F. Characterization of Indium Phosphide Quantum Dot Growth Intermediates Using MALDI-TOF Mass Spectrometry. *J. Am. Chem. Soc.* **2016**, *138*, 13469–13472.
- (85) Sakamoto, M.; Inoue, K.; Okano, M.; Saruyama, M.; Kim, S.; So, Y.-G.; Kimoto, K.; Kanemitsu, Y.; Teranishi, T. Light-stimulated carrier dynamics of CuInS2/CdS heterotetrapod nanocrystals. *Nanoscale* **2016**, *8*, 9517–9520.

- (86) Wu, K.; Liang, G.; Kong, D.; Chen, J.; Chen, Z.; Shan, X.; McBride, J. R.; Lian, T. Quasi-type II CuInS2/CdS core/shell quantum dots. *Chem. Sci.* **2016**, *7*, 1238–1244.
- (87) Li, L.; Pandey, A.; Werder, D. J.; Khanal, B. P.; Pietryga, J. M.; Klimov, V. I. Efficient Synthesis of Highly Luminescent Copper Indium Sulfide-Based Core/Shell Nanocrystals with Surprisingly Long-Lived Emission. *J. Am. Chem. Soc.* **2011**, *133*, 1176–1179.
- (88) Berends, A. C.; van der Stam, W.; Hofmann, J. P.; Bladt, E.; Meeldijk, J. D.; Bals, S.; de Mello Donega, C. Interplay between Surface Chemistry, Precursor Reactivity, and Temperature Determines Outcome of ZnS Shelling Reactions on CuInS2 Nanocrystals. *Chem. Mater.* 2018, 30, 2400–2413.
- (89) van der Stam, W.; Berends, A. C.; de Mello Donega, C. Prospects of Colloidal Copper Chalcogenide Nanocrystals. *Chem-PhysChem* **2016**, *17*, 559–581.
- (90) Xia, C.; Meeldijk, J. D.; Gerritsen, H. C.; de Mello Donega, C. Highly Luminescent Water-Dispersible NIR-Emitting Wurtzite CuInS2/ZnS Core/Shell Colloidal Quantum Dots. *Chem. Mater.* **2017**, 29, 4940–4951.
- (91) Kolny-Olesiak, J.; Weller, H. Synthesis and Application of Colloidal CuInS2 Semiconductor Nanocrystals. *ACS Appl. Mater. Interfaces* **2013**, *5*, 12221–12237.
- (92) Sandroni, M.; Wegner, K. D.; Aldakov, D.; Reiss, P. Prospects of Chalcopyrite-Type Nanocrystals for Energy Applications. *ACS Energy Lett.* **2017**, *2*, 1076–1088.
- (93) Leach, A. D. P.; Macdonald, J. E. Optoelectronic Properties of CuInS2 Nanocrystals and Their Origin. *J. Phys. Chem. Lett.* **2016**, 7, 572–583.
- (94) Deng, D.; Chen, Y.; Cao, J.; Tian, J.; Qian, Z.; Achilefu, S.; Gu, Y. High-Quality CuInS2/ZnS Quantum Dots for In vitro and In vivo Bioimaging. *Chem. Mater.* **2012**, *24*, 3029–3037.
- (95) Zhong, H.; Zhou, Y.; Ye, M.; He, Y.; Ye, J.; He, C.; Yang, C.; Li, Y. Controlled Synthesis and Optical Properties of Colloidal Ternary Chalcogenide CuInS2 Nanocrystals. *Chem. Mater.* **2008**, *20*, 6434–6443.
- (96) Whitham, P. J.; Knowles, K. E.; Reid, P. J.; Gamelin, D. R. Photoluminescence Blinking and Reversible Electron Trapping in Copper-Doped CdSe Nanocrystals. *Nano Lett.* **2015**, *15*, 4045–4051.
- (97) Nelson, H. D.; Li, X.; Gamelin, D. R. Computational Studies of the Electronic Structures of Copper-Doped CdSe Nanocrystals: Oxidation States, Jahn—Teller Distortions, Vibronic Bandshapes, and Singlet—Triplet Splittings. *J. Phys. Chem. C* **2016**, *120*, 5714—5723.
- (98) Knowles, K. E.; Hartstein, K. H.; Kilburn, T. B.; Marchioro, A.; Nelson, H. D.; Whitham, P. J.; Gamelin, D. R. Luminescent Colloidal Semiconductor Nanocrystals Containing Copper: Synthesis, Photophysics, and Applications. *Chem. Rev.* **2016**, *116*, 10820–10851.
- (99) Knowles, K. E.; Nelson, H. D.; Kilburn, T. B.; Gamelin, D. R. Singlet—Triplet Splittings in the Luminescent Excited States of Colloidal Cu+:CdSe, Cu+:InP, and CuInS2 Nanocrystals: Charge-Transfer Configurations and Self-Trapped Excitons. *J. Am. Chem. Soc.* **2015**, *137*, 13138—13147.
- (100) Marchioro, A.; Whitham, P. J.; Knowles, K. E.; Kilburn, T. B.; Reid, P. J.; Gamelin, D. R. Tunneling in the Delayed Luminescence of Colloidal CdSe, Cu+-Doped CdSe, and CuInS2 Semiconductor Nanocrystals and Relationship to Blinking. *J. Phys. Chem. C* **2016**, *120*, 27040–27049.
- (101) Kirkwood, N.; De Backer, A.; Altantzis, T.; Winckelmans, N.; Longo, A.; Antolinez, F. V.; Rabouw, F. T.; De Trizio, L.; Geuchies, J. J.; Mulder, J. T.; Renaud, N.; Bals, S.; Manna, L.; Houtepen, A. J. Locating and Controlling the Zn Content in In(Zn)P Quantum Dots. *Chem. Mater.* **2020**, 32, 557–565.
- (102) Janke, E. M.; Williams, N. E.; She, C.; Zherebetskyy, D.; Hudson, M. H.; Wang, L.; Gosztola, D. J.; Schaller, R. D.; Lee, B.; Sun, C.; Engel, G. S.; Talapin, D. V. Origin of Broad Emission Spectra in InP Quantum Dots: Contributions from Structural and Electronic Disorder. *J. Am. Chem. Soc.* **2018**, *140*, 15791–15803.
- (103) Gentle, C.; Wang, Y.; Haddock, T. N.; Dykstra, C. P.; van der Veen, R. M. Internal Atomic-scale Structure Determination and Band

- Alignment of II-VI Quantum Dot Heterostructures. J. Phys. Chem. C 2020, 124, 3895–3904.
- (104) Pedetti, S.; Ithurria, S.; Heuclin, H.; Patriarche, G.; Dubertret, B. Type-II CdSe/CdTe Core/Crown Semiconductor Nanoplatelets. *J. Am. Chem. Soc.* **2014**, *136*, 16430–16438.
- (105) de Mello Donegá, C. Formation of nanoscale spatially indirect excitons: Evolution of the type-II optical character of CdTe/CdSe heteronanocrystals. *Phys. Rev. B: Condens. Matter Mater. Phys.* **2010**, *81*, 165303.
- (106) Stein, J. L.; Mader, E. A.; Cossairt, B. M. Luminescent InP Quantum Dots with Tunable Emission by Post-Synthetic Modification with Lewis Acids. *J. Phys. Chem. Lett.* **2016**, *7*, 1315–1320.
- (107) Utterback, J. K.; Ruzicka, J. L.; Hamby, H.; Eaves, J. D.; Dukovic, G. Temperature-Dependent Transient Absorption Spectroscopy Elucidates Trapped-Hole Dynamics in CdS and CdSe Nanorods. J. Phys. Chem. Lett. 2019, 10, 2782–2787.
- (108) Krause, M. M.; Kambhampati, P. Linking surface chemistry to optical properties of semiconductor nanocrystals. *Phys. Chem. Chem. Phys.* **2015**, *17*, 18882–18894.
- (109) Kilina, S. V.; Tamukong, P. K.; Kilin, D. S. Surface Chemistry of Semiconducting Quantum Dots: Theoretical Perspectives. *Acc. Chem. Res.* **2016**, *49*, 2127–2135.
- (110) Wei, H. H.-Y.; Evans, C. M.; Swartz, B. D.; Neukirch, A. J.; Young, J.; Prezhdo, O. V.; Krauss, T. D. Colloidal Semiconductor Quantum Dots with Tunable Surface Composition. *Nano Lett.* **2012**, *12*, 4465–4471.
- (111) Cline, R. P.; Utterback, J. K.; Strong, S. E.; Dukovic, G.; Eaves, J. D. On the Nature of Trapped-Hole States in CdS Nanocrystals and the Mechanism of Their Diffusion. *J. Phys. Chem. Lett.* **2018**, *9*, 3532–3537
- (112) Veamatahau, A.; Jiang, B.; Seifert, T.; Makuta, S.; Latham, K.; Kanehara, M.; Teranishi, T.; Tachibana, Y. Origin of surface trap states in CdS quantum dots: relationship between size dependent photoluminescence and sulfur vacancy trap states. *Phys. Chem. Chem. Phys.* **2015**, *17*, 2850–2858.
- (113) Boldt, K.; Bartlett, S.; Kirkwood, N.; Johannessen, B. Quantification of Material Gradients in Core/Shell Nanocrystals Using EXAFS Spectroscopy. *Nano Lett.* **2020**, *20*, 1009–1017.